



Author Index of Volume A63

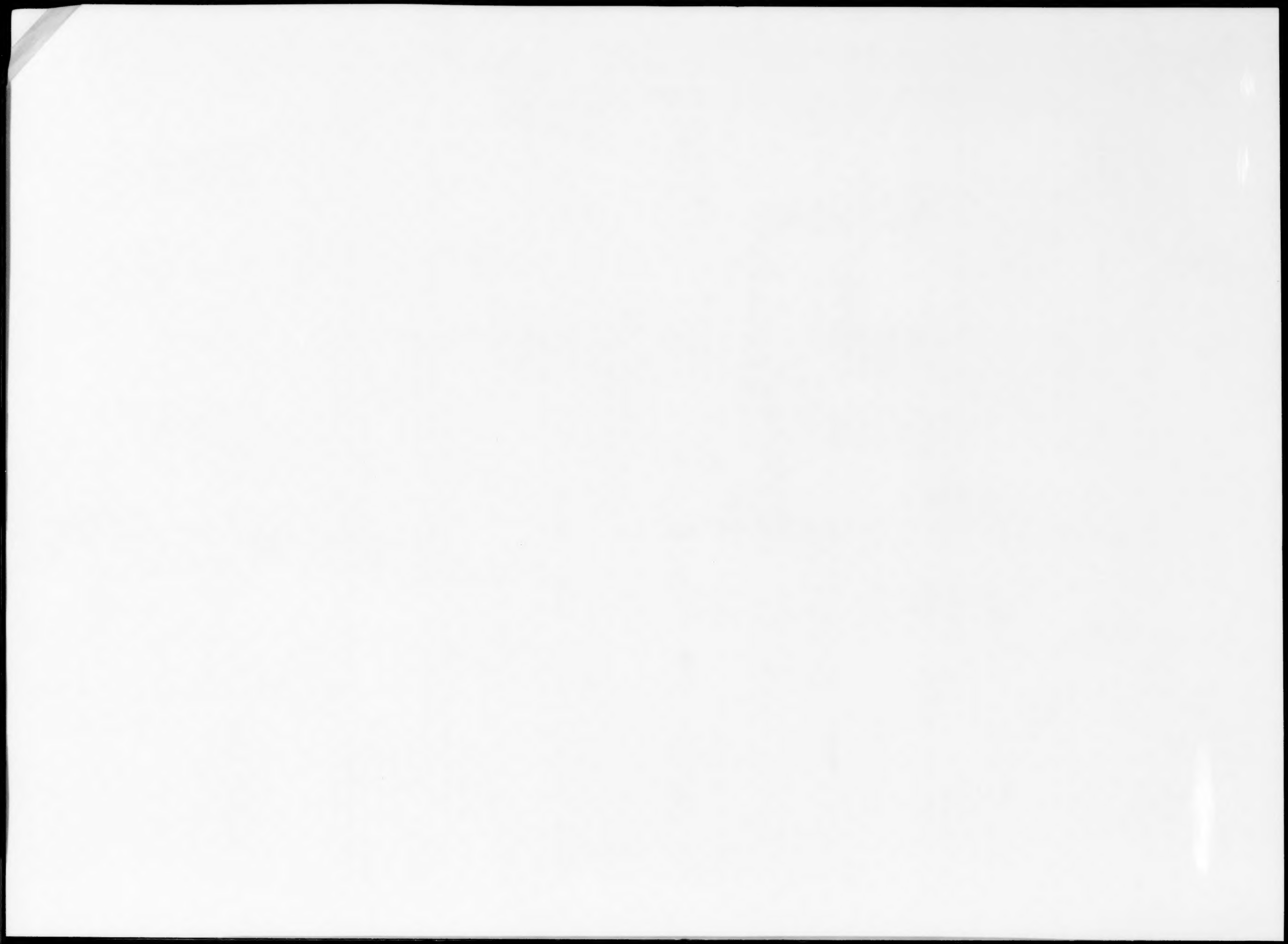
- Ansari, F., 177
Bao, M., 1, 19, 217
Beerschwinger, U., 229
Benoit, D., 251
Bergveld, P., 97, 163
Buchanan, R.C., 33
Cattan, E., 91
Chahoud, M., 141
Chao, L.-P., 105
Chen, H., 19, 217
Chen, K.-T., 105
Cheng, Y.C., 147, 223
Choi, W.K., 243
Chong, C.W., 243
Cunningham, M.J., 125, 135
Damjanovic, D., 153
Delaunay, G., 7
Devos, F., 205
Estève, D., 183
Fan, S., 169
Femuri, H., 7
Fisher, N.E., 27, 119
Fox, G.R., 153
Gaub, H.E., 47
Grattan, K.T.V., 85, 113, 197
Hardcastle, B.M., 61
Hofmann, U.G., 47
Hök, B., 69
Hu, Y.L., 85
Huang, M.Q., 223
Jaber, B., 91
Jackson, D.A., 27, 119
Jakšić, A., 129
Jenkins, D.F.L., 125, 135
Khalid, M.A.Hj., 125
Lai, P.T., 147, 223
Lawes, R.A., 61
Lee, M.H., 169
Li, B., 147
Li, G.Q., 223
Li, X., 1, 217
Li, Z., 209
Linde, H., 251
Liu, B.Y., 147
Liu, G., 169
Liu, L., 209
Ludden, B.P., 15
Meggett, B.T., 85
Meijerink, M.G.H., 163
Moineau, A., 7
Hofmann, U.G., 47
Ning, Y.N., 113
Olthuis, W., 97, 163
Owicki, J.C., 47
Palmer, A.W., 85, 113
Parak, W.J., 47
Pechstein, T., 191
Pedersen, M., 97, 163
Pejović, M., 129
Reid, D.J.C., 15
Remiens, D., 91, 135
Reuben, R.L., 229
Ristić, G., 129
Robertson, P.A., 15
Romare, D., 197
Rossi, C., 183
Rule, J., 15
Zeng, S.H., 223
Zhang, W., 113
Zhang, Z.Y., 85
Zheng, X.R., 147
Zhu, H., 19
Zou, Q., 209
Smith, L., 69
Sorge, S., 191
Strandman, C., 69
Sundeen, J.E., 33
Syms, R.R.A., 61
Tenerz, L., 69
Thierry, B., 91
Thong, J.T.L., 243
Tronc, P., 91
Velu, G., 135
Wajid, A., 41
Wang, C., 205
Wehmann, H.-H., 141
Whiting, C., 251
Woolsey, G.A., 27, 119
Yang, S.J., 229
Yuan, L., 177

Subject Index of Volume A63

- Accelerometers
a piezoresistive accelerometer with a novel vertical beam structure, 19
- Acoustic detection
Bragg grating in a two-mode optical fibre for sensing applications, 15
- Adaptive filtering
evaluation of different adaptive filtering techniques applied to white-light interferometric sensor systems, 197
- Anisotropic etching
a production process of silicon sensor elements for a fibre-optic pressure sensor, 69
- anisotropic-etching simulation of InP and Si, 141
- Beams
finite-element modelling and simulation on frequency characteristics of the silicon beam resonator attached to an E-type round diaphragm for measuring the concentrated force, 169
- Bulk-glass current sensors
tuning a bulk-glass optical current sensor by controlling conditions external to its reflecting surfaces, 27
- Faraday current sensors and the significance of subtended angles, 119
- Bulk micromachining
bulk micromachined silicon comb-drive electrostatic actuators with diode isolation, 61
- Capacitance
study on linearization of silicon capacitive pressure sensors, 1
- Capacitive sensors
an IC-compatible polyimide pressure sensor with capacitive readout, 163
- Ceramics
characterization of ferroelectric and piezoelectric properties of lead titanate thin films deposited on Si by sputtering, 91
- Cermet films
electrical properties of nickel-zirconia cermet films for temperature- and flow-sensor applications, 33
- Comb-drive electrostatic actuators
bulk micromachined silicon comb-drive electrostatic actuators with diode isolation, 61
- Composite films
electrical properties of nickel-zirconia cermet films for temperature- and flow-sensor applications, 33
- Condenser microphones
theoretical and experimental studies of single-chip-processed miniature silicon condenser microphone with corrugated diaphragm, 209
- Conduction percolation
electrical properties of nickel-zirconia cermet films for temperature- and flow-sensor applications, 33
- Corrugated diaphragms
theoretical and experimental studies of single-chip-processed miniature silicon condenser microphone with corrugated diaphragm, 209
- CVD oxide
PMOS dosimetric transistors with two-layer gate oxide, 129
- Decay-time thermometry
ruby-based decay-time thermometry: effect of probe size on extended measurement range (77–800 K), 85
- Deconvolution
the use of some iterative deconvolution algorithms to improve the spatial resolution of a flat magnetic sensor, 7
- Dielectric membranes
theoretical and experimental study of silicon micromachined micro-heater with dielectric stacked membranes, 183
- Differential sensors
an IC-compatible polyimide pressure sensor with capacitive readout, 163
- Diode isolation
bulk micromachined silicon comb-drive electrostatic actuators with diode isolation, 61
- Electrostatic actuation
cantilever vibration control by electrostatic actuation for magnetic force microscopy, 125
- Etch characteristics
etch characteristics of various materials in ethanolamine etchants, 251
- Etching parameters
TMAH etching of silicon and the interaction of etching parameters, 243
- Etching simulation
anisotropic-etching simulation of InP and Si, 141
- Ethanolamine etchants
etch characteristics of various materials in ethanolamine etchants, 251
- E-type round diaphragms
finite-element modelling and simulation on frequency characteristics of the silicon beam resonator attached to an E-type round diaphragm for measuring the concentrated force, 169
- Fading
PMOS dosimetric transistors with two-layer gate oxide, 129
- Faraday current sensors
Faraday current sensors and the significance of subtended angles, 119
- Ferroelectric properties
characterization of ferroelectric and piezoelectric properties of lead titanate thin films deposited on Si by sputtering, 91
- Fiber optics
white-light interferometric fiber-optic distributed strain-sensing system, 177
- Fiber-optic thermometers
ruby-based decay-time thermometry: effect of probe size on extended measurement range (77–800 K), 85
- Fibre Bragg gratings
Bragg grating in a two-mode optical fibre for sensing applications, 15
- Finite-element method
finite-element modelling and simulation on frequency characteristics of the silicon beam resonator attached to an E-type round diaphragm for measuring the concentrated force, 169

- Flow sensors
electrical properties of nickel-zirconia cermet films for temperature- and flow-sensor applications, 33
- Fluorescence lifetime
ruby-based decay-time thermometry: effect of probe size on extended measurement range (77–800 K), 85
- Force
finite-element modelling and simulation on frequency characteristics of the silicon beam resonator attached to an E-type round diaphragm for measuring the concentrated force, 169
- Force sensitivity evaluation
shape optimal design and force sensitivity evaluation of six-axis force sensors, 105
- Force sensors
shape optimal design and force sensitivity evaluation of six-axis force sensors, 105
- Friction
frictional study of micromotor bearings, 229
- Gas chromatography
fully integrated thermal conductivity sensor for gas chromatography without dead volume, 191
- Gas sensors
fully integrated thermal conductivity sensor for gas chromatography without dead volume, 191
- Guide-wire fibre-optic pressure sensors
a production process of silicon sensor elements for a fibre-optic pressure sensor, 69
- Humidity sensitivity
photo-, thermal and humidity sensitivity characteristics of $\text{Sr}_{1-x}\text{La}_x\text{TiO}_3$ film on SiO_2/Si substrate, 223
- IC-compatible sensors
a silicon condenser microphone with polyimide diaphragm and back-plate, 97
- Indium phosphide
anisotropic-etching simulation of InP and Si, 141
- Integrated sensors
an integrated PVDF ultrasonic sensor with improved sensitivity using polyimide, 147
- an IC-compatible polyimide pressure sensor with capacitive readout, 163
- Interface traps
PMOS dosimetric transistors with two-layer gate oxide, 129
- Iterative algorithms
the use of some iterative deconvolution algorithms to improve the spatial resolution of a flat magnetic sensor, 7
- Lateral acceleration
a piezoresistive accelerometer with a novel vertical beam structure, 19
- Lateral resolution
lateral resolution of light-addressable potentiometric sensors: an experimental and theoretical investigation, 47
- Lead titanate
characterization of ferroelectric and piezoelectric properties of lead titanate thin films deposited on Si by sputtering, 91
- Light-addressable potentiometric sensors (LAPSSs)
lateral resolution of light-addressable potentiometric sensors: an experimental and theoretical investigation, 47
- Light-pulse detectors
a cumulative differential light-pulse detector using source-coupled MOS current switches, 205
- Linearity
study on linearization of silicon capacitive pressure sensors, 1
- Magnetic force microscopy
cantilever vibration control by electrostatic actuation for magnetic force microscopy, 125
- Maskless etching
a novel micromachining technology for multilevel structures of silicon, 217
- Microactuators
the use of sputtered ZnO piezoelectric thin films as broad-band microactuators, 135
- Microheaters
theoretical and experimental study of silicon micromachined micro-heater with dielectric stacked membranes, 183
- Micromachining
a piezoresistive accelerometer with a novel vertical beam structure, 19
- Micromotor bearings
frictional study of micromotor bearings, 229
- Microsensors
finite-element modelling and simulation on frequency characteristics of the silicon beam resonator attached to an E-type round diaphragm for measuring the concentrated force, 169
- MOS current switches
a cumulative differential light-pulse detector using source-coupled MOS current switches, 205
- Optical current-measurement systems
analysis of the effect of vibration-induced noise in different fibre leads used in an optical current-measurement system, 113
- Optical current sensors
Faraday current sensors and the significance of subtended angles, 119
- Optical fibres
electrical characterization of sputter-deposited ZnO coatings on optical fibers, 153
- Optimal design
shape optimal design and force sensitivity evaluation of six-axis force sensors, 105
- Oxide trapped charge
PMOS dosimetric transistors with two-layer gate oxide, 129
- Photosensitivity
photo-, thermal and humidity sensitivity characteristics of $\text{Sr}_{1-x}\text{La}_x\text{TiO}_3$ film on SiO_2/Si substrate, 223
- Piezoelectric optical-fiber coatings
electrical characterization of sputter-deposited ZnO coatings on optical fibers, 153
- Piezoelectric properties
characterization of ferroelectric and piezoelectric properties of lead titanate thin films deposited on Si by sputtering, 91
- Piezoelectric thin films
the use of sputtered ZnO piezoelectric thin films as broad-band microactuators, 135
- electrical characterization of sputter-deposited ZnO coatings on optical fibers, 153
- {100} Planes
a production process of silicon sensor elements for a fibre-optic pressure sensor, 69
- PMOS dosimeters
PMOS dosimetric transistors with two-layer gate oxide, 129
- Polyimide
a silicon condenser microphone with polyimide diaphragm and back-plate, 97
- an integrated PVDF ultrasonic sensor with improved sensitivity using polyimide, 147

- an IC-compatible polyimide pressure sensor with capacitive readout, 163
- Potassium hydroxide
a production process of silicon sensor elements for a fibre-optic pressure sensor, 69
- Pressure sensors
study on linearization of silicon capacitive pressure sensors, 1
an IC-compatible polyimide pressure sensor with capacitive readout, 163
- Quartz-crystal microbalances
on the accuracy of the quartz-crystal microbalance (QCM) in thin-film depositions, 41
- Radial resonance
electrical characterization of sputter-deposited ZnO coatings on optical fibers, 153
- Reactive sputtering
electrical characterization of sputter-deposited ZnO coatings on optical fibers, 153
- Restoration of sensor images
the use of some iterative deconvolution algorithms to improve the spatial resolution of a flat magnetic sensor, 7
- Ruby
ruby-based decay-time thermometry: effect of probe size on extended measurement range (77–800 K), 85
- Sensitivity
PMOS dosimetric transistors with two-layer gate oxide, 129
- Silicon
study on linearization of silicon capacitive pressure sensors, 1
bulk micromachined silicon comb-drive electrostatic actuators with diode isolation, 61
characterization of ferroelectric and piezoelectric properties of lead titanate thin films deposited on Si by sputtering, 91
anisotropic-etching simulation of InP and Si, 141
TMAH etching of silicon and the interaction of etching parameters, 243
- Silicon condenser microphones
a silicon condenser microphone with polyimide diaphragm and back-plate, 97
- Silicon etch
a novel micromachining technology for multilevel structures of silicon, 217
- Single-chip fabrication
theoretical and experimental studies of single-chip-processed miniature silicon condenser microphone with corrugated diaphragm, 209
- $\text{Sr}_{1-x}\text{La}_x\text{TiO}_3$ thin films
photo-, thermal and humidity sensitivity characteristics of $\text{Sr}_{1-x}\text{La}_x\text{TiO}_3$ film on SiO_2/Si substrate, 223
- Strain gages
shape optimal design and force sensitivity evaluation of six-axis force sensors, 105
- Strain sensors
white-light interferometric fiber-optic distributed strain-sensing system, 177
- Subtended angles
Faraday current sensors and the significance of subtended angles, 119
- Temperature coefficient of resistance
electrical properties of nickel-zirconia cermet films for temperature- and flow-sensor applications, 33
- Tetramethylammonium hydroxide (TMAH)
TMAH etching of silicon and the interaction of etching parameters, 243
- Thermal conductivity detectors
fully integrated thermal conductivity sensor for gas chromatography without dead volume, 191
- Thermal optimization
theoretical and experimental study of silicon micromachined microheater with dielectric stacked membranes, 183
- Thermal sensitivity
photo-, thermal and humidity sensitivity characteristics of $\text{Sr}_{1-x}\text{La}_x\text{TiO}_3$ film on SiO_2/Si substrate, 223
- Thin films
on the accuracy of the quartz-crystal microbalance (QCM) in thin-film depositions, 41
- Tuning
tuning a bulk-glass optical current sensor by controlling conditions external to its reflecting surfaces, 27
- Ultrasonic transducers
an integrated PVDF ultrasonic sensor with improved sensitivity using polyimide, 147
- Vibration control
cantilever vibration control by electrostatic actuation for magnetic force microscopy, 125
- Vibration-induced noise
analysis of the effect of vibration-induced noise in different fibre leads used in an optical current-measurement system, 113
- White-light interferometry
white-light interferometric fiber-optic distributed strain-sensing system, 177
evaluation of different adaptive filtering techniques applied to white-light interferometric sensor systems, 197
- Zinc oxide
the use of sputtered ZnO piezoelectric thin films as broad-band microactuators, 135
electrical characterization of sputter-deposited ZnO coatings on optical fibers, 153
- Z-match technique
on the accuracy of the quartz-crystal microbalance (QCM) in thin-film depositions, 41



1